Massively parallel functional testing of *MSH2* missense variants conferring Lynch Syndrome risk

Xiaoyan Jia,[1] Bala Bharathi Burugula,[1] Victor Chen.[1] Rosemary M. Lemons,[1] Sajini Jayakody,[1] Mariam Maksutova,[1] Jacob O. Kitzman[1,2,*]

[1]Department of Human Genetics, University of Michigan, Ann Arbor, MI, 48109, USA

[2]Department of Computational Medicine & Bioinformatics, University of Michigan, Ann Arbor, MI, 48109, USA

*correspondence: kitzmanj@umich.edu

Abstract

The lack of functional evidence for the majority of missense variants limits their clinical interpretability, and poses a key barrier to the broad utility of carrier screening. In Lynch Syndrome (LS), one of the most highly prevalent cancer syndromes, nearly 90% of clinically observed missense variants are deemed “variants of uncertain significance” (VUS). To systematically resolve their functional status, we performed a massively parallel screen in human cells to identify loss-of-function missense variants in the key DNA mismatch repair factor *MSH2*. The resulting functional effect map is substantially complete, covering 94% of the 17,746 possible variants, and is highly concordant (96%) with existing functional data and expert clinicians’ interpretations. The large majority (89%) of missense variants were functionally neutral, perhaps unexpectedly in light of its evolutionary conservation. These data provide ready-to-use functional evidence to resolve the ~1,300 extant missense VUSs in *MSH2*, and may facilitate the prospective classification of newly discovered variants in the clinic.

Introduction

28 Lynch Syndrome (OMIM:120435), the first discovered familial cancer syndrome[1], confers
29 predisposition to colorectal and endometrial cancers due to loss of DNA mismatch repair (MMR) and the
30 resulting mutagenic burden[2–5]. Most affected individuals inherit a single loss-of-function variant in one of
31 four MMR factors (*MSH2, MLH1, MSH6, PMS2*), followed by a somatic 'second hit' inactivating the
32 remaining functional copy. Due to high prevalence in the general population (≥1:300)[6,7], clear genetic
33 etiology, and potential for prevention through intensified surveillance, pathogenic MMR gene variants are
34 considered clinically actionable[8]. Though screening for MMR gene variants is increasingly routine,
35 accurately interpreting them imposes a substantial clinical burden.
36
37 Missense changes together comprise 20-30% of Lynch Syndrome variants[9], and are particularly
38 challenging to interpret: their functional impacts may range from minimal to profound, and as most are
39 individually rare, prior evidence to guide their classification is frequently unavailable. Compounding this,
40 variants which inactivate MMR exhibit incomplete penetrance, conferring a lifetime cancer risk between
41 15% and 60% depending upon which gene is inactivated[10,11]. Consequently, MMR gene missense variants
42 are not readily ruled in or out as casual, even when observed in an individual with a relevant cancer
43 diagnosis. Indeed, the overwhelming majority of Lynch Syndrome gene missense variants listed in ClinVar
44 (4,762/5,473, 87.0%) are deemed "variants of uncertain significance", or VUS (Figure S1), and cannot be
45 used to guide diagnosis and management.
46
47 Functional studies can provide a key source of evidence to support variant classification[12,13].
48 Traditionally, these studies are conducted *post hoc* and cannot be completed within the timeframe needed
49 to support real-time interpretation. The heterogeneity of the functional data accumulated in the literature
50 for MMR gene variants poses a further barrier, as the model systems and assays in use vary widely. Some
51 assays interrogate specific mechanistic details (e.g., ATPase activity), while others report the end result
52 upon *de novo* mutation rate. Human MMR variants have been extensively modeled in budding yeast[14,15],
53 but not every human MMR factor complements its yeast ortholog[16], and many human variants occur
54 outside of well-conserved domains and so are not readily modeled on diverged orthologs. Reconstituting

55 MMR *in vitro* enables mechanistic studies, but may not reflect functional state under physiological
56 conditions. Thus, while individual functional reports on MMR gene variants abound, it remains a challenge
57 to bring this disparate body of evidence to bear on the task of classifying variant pathogenicity.
58
59 To address these challenges, we applied deep mutational scanning[17] to prospectively and
60 systematically measure the functional impact of missense variants in the major Lynch Syndrome gene
61 *MSH2.* We developed human cell line models in which *MSH2* deletion was complemented by libraries of
62 variants comprising nearly every possible *MSH2* missense allele. We leveraged an established chemical
63 selection for mismatch repair dysfunction[18–21], and used deep sequencing to identify the surviving *MSH2*
64 variants. The resulting missense loss-of-function (LOF) scores are highly concordant with existing
65 functional data and substantially outperform bioinformatic variant effect predictions. We observe that adult
66 populations are significantly depleted for deleterious missense *MSH2* mutations, akin to what is observed
67 for whole-gene deletions and truncating point variants in MMR genes[22,23]. These data provide a uniformly
68 generated set of functional evidence, calibrated against known standards of pathogenicity, and will assist
69 the interpretation of variants which would otherwise remain a source of uncertainty for clinicians, patients,
70 and their relatives.
71

72 ## Material and Methods

73

74 ### *MSH2* knockout cell lines

75 Clonal knockout cell lines (Figure S2) were derived by transient transfection with plasmids expressing
76 SpCas9 and guide RNAs targeting *MSH2*. For HAP1, a single guide sequence (primers JBW0001/2)
77 targeting *MSH2* exon 6 was cloned into pSpCas9(BB)-2A-GFP (PX458, Addgene #48138) as described[24].
78 For HEK293, four guides (primers VC0019/20, VC0021/22, VC0023/24, VC0027/28), two flanking each
79 side of the *MSH2* locus, were each likewise cloned into pSpCas9(BB)-2A-PuroV2 (PX459, Addgene
80 #62988)[24] and used in combination. Wild-type HAP1 or HEK293 cells were transfected with the respective
81 plasmid(s) using Lipofectamine 3000 (Thermo). Clonal HAP1 *MSH2* knockout cells were isolated by sorting

82 single GFP positive cells using a FACS Aria II instrument (BD), and colonies were screened for *MSH2*
83 exon 6 frameshift mutations. Clonal HEK293 *MSH2* knockout cells were isolated by dilution, expanded,
84 and screened by PCR for the presence of a full-gene knockout deletion junction(s), and the absence of an
85 internal target in exon 12.
86
87 ***MSH2* cloning**
88 Wild-type *MSH2* cDNA was PCR amplified from a lentiORF plasmid (Dharmacon OHS5897), and fused
89 in-frame by HiFi Assembly (NEB) to a blasticidin resistance marker amplified from pLentiCas9Blast
90 (AddGene #52962), separated by a P2A self-cleaving peptide linker (Figure S3). The p.Ala636Pro mutation
91 was introduced by site-directed mutagenesis. Each resulting construct was subcloned a doxycycline-
92 inducible lentiviral expression plasmid (pCW57.1, Addgene #41393) by digestion with SalI and NheI and
93 ligation with T4 DNA ligase (NEB).
94
95 **Western blotting**
96 Cells were seeded on 6-well plates, grown to confluence, and lysed by the addition of RIPA buffer and
97 protease inhibitor cocktail (Sigma-Aldrich). Protein extracts were run for 30 min at 200 V on denaturing
98 Bolt 4-12% Bis-Tris Plus Gels in 1× Bolt MOPS SDS buffer (Invitrogen), transferred to a nitrocellulose
99 membrane for 1.5 h at 10 V, and blocked at 4˚C overnight in 1X TBST (20 mM Tris base, 0.15 M NaCl,
100 0.1% Tween-20, 2% milk). Blots were probed with a 1:2000 dilution of anti-MSH2 (FE11, Thermo) and as
101 loading control, 1:5000 dilution of anti-beta actin (BA3R, Invitrogen), followed by a 1:1000 dilution of HRP-
102 conjugated goat anti-mouse IgG (H+L) secondary antibody (#62-6520, Invitrogen). Detection was
103 performed with SuperSignal West Pico Chemiluminescent substrate (Thermo) and ChemiDoc XRS system
104 (BioRad).
105
106 **Cell culture**
107 Human HAP1 cells (Horizon Discovery) were cultured in IMDM and HEK293 and 293T/17 cells (ATCC)
108 were cultured in DMEM, each supplemented with 10% fetal bovine serum, 100 U/ml penicillin and 100 g/ml

109 streptomycin. During routine passaging, cells were washed with PBS pH 7.4 and dissociated with TrypLE
110 Express. Cell lines were tested monthly for mycoplasma; all were negative.
111
112 **Library mutagenesis**
113 *MSH2* cDNA was divided into 21 tiles (Table S1), and each was subjected to programmed allelic series
114 mutagenesis[25] modified as follows. Mutagenic PCR reactions used PrimeStar GXL polymerase (Takara),
115 and 45mer mutagenesis primers (Table S2) were individually synthesized. Each codon was randomized
116 in an individual PCR (program MUT_1, Table S3), with a common forward primer (JOK_0184) upstream
117 of *MSH2,* and a codon-specific degenerate (NNN) reverse primer. Resulting partial-length mutant cDNA
118 was subjected to 10 cycles of strand extension (program MUT_2) with limiting template (250 pg) of wild-
119 type cDNA plasmid. Finally, each full-length mutant cDNA was PCR amplified with flanking outer primers
120 (program MUT_3, primers JOK_0184 and JOK_0185). Per-codon products were pooled within each tile
121 and purified by SPRI bead cleanup[26]. PCR products were digested with DpnI, to deplete starting plasmid,
122 and NheI-HF and SalI-HF, for cloning into the lentiviral vector as described above. Ligation products were
123 transformed into Endura electrocompetent *E. coli* (Lucigen). A small aliquot of the transformant culture was
124 plated to monitor library complexity, while the remainder was expanded for 12-16 hours at 32ºC in Luria
125 Broth with 100 ug/ml ampicillin (LB+amp). We required total colony forming units ≥ $4x10^4$, for mean ~10-
126 fold coverage per variant. Lentiviral tile plasmid libraries were isolated using ZymoPURE II Plasmid kit,
127 and converted to shotgun libraries for deep sequencing by Tn5 tagmentation[27], to assess mutational
128 specificity and coverage (Figure S4). Absent or under-represented codons were individually retrieved from
129 the earlier mutagenesis steps, pooled, cloned as above, and spiked into each tile library as needed to
130 equalize coverage. Finally, these mutant tile libraries, as well as control clones (WT and A636P), were
131 modified to add trackable barcodes. Each clone or library was linearized with SalI-HF (NEB) downstream
132 of the *MSH2*-2A-bl^R ORF, and a degenerate 20-mer (primer jklab0172) was inserted by HiFi Assembly
133 (NEB). The resulting barcoded clone pools were transformed, expanded, and isolated as described above.
134

135 **Lentiviral preparation and transduction**

136 Barcoded *MSH2*-2A-bl^R cDNA libraries were packaged into lentivirus by co-transfecting HEK293T/17 cells
137 (ATCC) with the transfer plasmid pool plus envelope and packaging vectors (pMD2.G, Addgene #12259
138 and psPAX2, #12260). For each pool, 4.4x10^6 cells were plated in a 100 mm dish, then transfected with
139 17 ug total plasmid (2.0:1.0:1.3 transfer:envelope:packaging ratio), using Lipofectamine 3000 (Thermo).
140 Media was replaced at 6 h post transfection, and viral supernatants were collected at 24 h, passed through
141 an 0.45 micron filter (Millipore), and used immediately or stored at -80ºC until use. Viral titer was estimated
142 by transduction with a dilution series followed by puromycin selection and CellTiterGlo (Promega) cell
143 proliferation assay[28], and verified by counting unique barcodes in the transduced population (barc-seq,
144 described below). For each tile, *MSH2* knockout HAP1 or HEK293 cells were transduced with mutant
145 library at low multiplicity of infection (< 0.1), by applying 1.5 ml viral supernatant (with 8 µg mL^{-1} polybrene)
146 to each of four 100mm dishes (Corning) containing ~7.5x10^6 cells. After 48 h, transduced cells were
147 selected by addition of 1 µg mL^{-1} puromycin, which was included in all subsequent steps.

148

149 **Mismatch repair functional selection**

150 Cells expressing loss-of-function *MSH2* variants were enriched by adding 6-thioguanine (6-TG) to the
151 culture media. To find an optimal concentration, parental and *MSH2* KO cell lines were plated in
152 quadruplicate wells of a 96-well plate and treated with a range of 6-TG concentrations. Cell growth after 4
153 days was measured using the CellTiterGlo 2 kit (Promega) and a GloMax luminometer (Promega), and
154 survival was normalized to untreated wells (Figure S2).

155

156 For library selections, each mutant tile cell population was spiked with barcoded knock-in control cells
157 (*MSH2* WT: to 10% of the population, A636P: to 0.5%), then split and expanded in triplicate 10 cm dishes
158 (Figure S5-S6) in media supplemented with 1 µg mL^{-1} doxycycline to induce *MSH2* expression. From each
159 baseline passage ("P0") culture, 10^7 cells were collected for gDNA extraction, and cells were split into 6-
160 TG treated and mock-treated cultures, with media containing 1 µg mL^{-1} puromycin, 1 µg mL^{-1} doxycycline,
161 5 µg mL^{-1} blasticidin (to enforce *MSH2* expression), with and without 1 uM 6-TG, respectively. Cells were

162 grown to confluence for two rounds, at each round harvesting ≥10^7 cells for gDNA extraction and seeding

163 with $3x10^6$ cells to avoid population bottlenecks.

164

165 **Amplification and sequencing of integrated *MSH2***

166 After selections, genomic DNA was isolated from 1-$3x10^7$ cells using the Quick-DNA Midiprep Plus kit, and

167 sequenced in tiles. To provide sufficiently redundant sampling of integrated *MSH2* libraries, for each

168 sample, 16 replicate PCR reactions were assembled, each with 0.5 µg of gDNA as template (template

169 copy number of $2.4x10^6$ genome equivalents per tile). Integrated inserts (~3.7 kbp), including *MSH2* cDNA

170 and associated barcode, were PCR amplified with PrimeSTAR GXL (program MSH2gDNA). Each set of

171 16 replicate amplicons was pooled and purified with SPRI beads. Next, tile-seq libraries were prepared

172 from each pool of amplified integrated *MSH2* constructs. Tile-specific primers (Table S2) were used to

173 further amplify the tile mutagenized in each sample in a PCR reaction (program TILESEQ) with 10 ng full-

174 length amplicon (≥ $2.6x10^9$ copies) as template. Dual-indexed illumina adapters (sequences available upon

175 request) were then added by a subsequent round of PCR. The resulting short amplicon libraries thus

176 provide overlapping read coverage for most of each tile. Tile-seq libraries were pooled for paired end 150bp

177 Illumina sequencing (≥ $1x10^6$ paired reads per sample, n=189 libraries). Pool complexity (the number of

178 distinct transduced clones) was assessed by tile-seq (Figure S7) and barc-seq (Figure S8). Barcodes were

179 amplified from the full-length *MSH2* amplicon and converted to illumina amplicon libraries, as for tile-seq,

180 but using primers jklab0077 and jklab0078 (program BCSEQ) . Each tile's starting population ("P0") had

181 ≥20,000 barcodes, indicating at least that number of unique initial transduction events. Catalogs of

182 barcodes associated with each of the two *MSH2* control clones (WT, A636P), and for each tile library, were

183 established by barc-seq (as described above) from their respective gDNAs at P0 (after transduction).

184 Finally, tile-seq libraries were prepared from a fully wild-type *MSH2* clone plasmid DNA, to measure and

185 correct position-specific errors, primarily single base substitutions which varied considerably by position
186 and type (Figure S9)
187
188 **Sequence data processing**
189 Shotgun sequencing reads were aligned to a set of *MSH2* cDNA sequences with each codon sequentially
190 replaced with "NNN" using bbmap (https://jgi.doe.gov/data-and-tools/bbtools/) in semi-perfect mode, to
191 identify reads containing at most one mutated codon with between one and three edits. Custom python
192 scripts converted the resulting alignments to a per-sample table of counts for every possible codon
193 mutation. For tile-seq libraries, paired reads were overlapped and error-corrected with PEAR v0.9.6[29];
194 only perfectly matching pairs were used. For each tile, all possible single-codon mutation sequences were
195 enumerated, and the count of reads exactly matching each mutant sequence was tabulated. Reads with
196 additional mutations or sequencing errors were discarded. Barc-seq reads were clustered with starcode
197 v1.3[30] to define and count unique barcodes. To determine the number of distinct barcodes present, robust
198 to sequencing or amplification artifacts, we ranked clustered barcode groups by read count and determined
199 the minimum number of barcodes for which all equally or more abundant barcodes cumulatively accounted
200 for ≥90% of the total read counts.
201
202 **Variant enrichment scoring**
203 The raw frequency of each per codon mutation *i* in each sample *s* was calculated, with a pseudocount of
204 0.9: $f'_{i,s} = \frac{(c_{i,s}+0.9)}{\sum_k (c_{k,s}+0.9)}$. Position specific error rates from wild-type *MSH2* plasmid tile-seq were subtracted
205 and normalized to yield corrected frequencies: $f_{i,s} = \frac{max\,(f'_{i,s}-f'_{i,WT},0)}{\sum_k max\,(f'_{k,s}-f'_{k,WT},0)}$. Variants with frequency
206 ≤1/200,000 in the initial transduced cell population (P0) were removed from further analysis. Next, variants
207 substantially enriched or depleted after mock treatment (absolute $\log_2$ ratio > 2, after two passages

208 blasticidin vs P0) were likewise removed; these variants may be *in cis* with a frameshift or premature
209 truncating mutation beyond the sequenced tile. A loss-of-function (LOF) score was taken as the $\log_2$ratio
210 of the frequency after 6-TG treatment over that after mock treatment. For amino acid substitutions
211 represented by more than one equivalent codon substitution, the median was taken across those codons'
212 LOF scores to yield an amino acid-level LOF score. Within each replicate, variants were removed when
213 represented by exactly two LOF scores with opposite signs. Finally, the median score was taken for each
214 amino acid LOF score across the three replicates; when only two replicate scores remained and had
215 discordant signs, they were removed. False discovery rate was estimated by random sampling of
216 synonymous variants' read counts, with replacement and keeping triplicates together. To mimic the
217 number of codons corresponding to a given mutant amino acid, synonymous variants were sampled in
218 groups of size one to six. Counts were processed to LOF scores and filtered as described above,
219 combining first within each simulated missense amino acid and then across replicates; final LOF scores
220 greater than zero were taken as false discoveries. Overall FDR was estimated as the mean FDR for amino
221 acids with each number of different variant codons (1, 2, 3, 4, or 6 codons), weighted by the fraction of
222 variant amino acids with that number of codons.
223
224 **Clinical and population variants**
225 *MSH2* missense variants and classifications were obtained from ClinVar
226 (https://www.ncbi.nlm.nih.gov/clinvar/) on 2020 April 14. Redundant variants were removed, and likely
227 splice-disruptive variants with a SpliceAI[31] score of ≥0.2 were filtered out, along with those where the
228 ClinVar record indicated a known splice-disruptive mechanism (Table S4). Only variants with expert panel
229 reviews were included in comparisons to LOF scores. *MSH2* missense variants and classifications were
230 accessed from InSiGHT (https://www.insight-group.org/variants/databases/). *MSH2* missense population
231 variation was obtained from the gnomAD database[23], combining whole-genome and exome calls from
232 versions 2.1.1 and 3.0. The expected number of LOF missense mutations was modeled with a binomial
233 distribution parameterized by n=744 (the number of scored missense variants in gnomAD) and p taken as

234 the sum of LOF missense point variants' relative likelihoods of occurring *de novo*[32], equivalent to drawing
235 sets of size 744 from the universe of possible missense SNVs with probabilities scaled by their individual
236 relative likelihoods.
237
238 **Bioinformatic classification**
239 All *MSH2* missense variants were scored by the following bioinformatic tools:CADD[33], PolyPhen-2[34],
240 REVEL[35], PON-MMR[36], MAPP-MMR[37], and FoldX (scores obtained from [38]). For CADD and REVEL,
241 scores were available only for missense variants reachable by single-base variants (SNVs); for amino-acid
242 substitutions that could arise from more than one SNV, the mean of those SNVs' scores was taken.
243
244 **MSH2 structure and conservation**
245 The MSH2 crystal structure[39] was obtained from the Protein Databank (accession 2O8E) and rendered
246 with PyMOL. Amino acid secondary structure assignment was extracted from pre-calculated DSSP files[40].
247 Surface accessibility was calculated using ASA (http://cib.cf.ocha.ac.jp/bitool/ASA/). MSH2 ortholog
248 protein sequences were downloaded from Ensembl (https://useast.ensembl.org/) and aligned with
249 MUSCLE[41].
250
251 **Results**
252
253 **A Human Cell Platform to Test *MSH2* Variant Function**
254
255 We established a human cell system to model *MSH2* variant function using the mismatch repair
256 proficient[42] cell line HAP1 (Figure 1A, C). First, to disrupt MMR, we derived clonal *MSH2* knockout cells
257 bearing a 19-bp frameshift deletion in *MSH2* exon 6, and verified that it lacked detectable MSH2 protein
258 expression (Figure S2). To restore MMR, we stably reintroduced into cells either wild-type *MSH2* cDNA
259 (KO+WT) or a pathogenic founder allele (KO+A636P) on inducible lentiviral constructs. After inducing

260 expression with doxycycline, wild-type MSH2 protein reached near-endogenous levels, while A636P was
261 only barely detectable, consistent with the known destabilizing effect of this variant[43] (Figure S3).
262
263 As a readout for *MSH2* function, we leveraged selection with the purine analog 6-thioguanine (6-
264 TG)[19,44]. Incorporation of 6-TG is selectively toxic to MMR-proficient cells, as it creates lesions that the
265 MMR machinery recognizes but cannot repair, culminating in replication arrest[20,21]. As expected, KO cells
266 showed increased 6-TG resistance compared to parental HAP1 cells, while 6-TG sensitivity was restored
267 by reintroduction of wild-type *MSH2* but not the pathogenic A636P mutant (Figures 1B and S5). To mimic
268 simultaneously testing thousands of mutations, we prepared a mixed culture of KO+WT cells and
269 KO+A636P cells, with the respective *MSH2* expression constructs bearing distinct, identifying barcode
270 libraries *in cis* (Figure S5). We quantified barcode abundances by deep sequencing (**Material and**
271 **Methods**), and found barcodes linked to the pathogenic variant A636P were strongly enriched relative to
272 WT barcodes (median fold change: 179, $P<2.2\times10^{-16}$, Kolmogorov-Smirnov test). This result confirms the
273 feasibility of highly multiplexed MMR functional tests in isogenic human cell mixtures.
274
275 **A Functional Effect Map Covering >17,000 *MSH2* Missense Variants**
276
277 To model known and novel *MSH2* variants, we applied single amino-acid saturation mutagenesis[25] to
278 generate libraries comprising every possible missense, synonymous and nonsense variant (**Material and**
279 **Methods**). *MSH2* cDNA (2,802 bp) was divided into 21 tiles to enable tracking by amplicon sequencing[45],
280 and to mitigate the impact of recombination during lentiviral replication[46]. The mutant cDNA library for each
281 tile was cloned into the inducible lentiviral vector mentioned above, followed by a C-terminal 2A linker and
282 a blasticidin resistance gene, to permit selection for complete in-frame cDNA expression (Figure S3). HAP1
283 *MSH2* KO cells were transduced at low multiplicity (<0.1) to yield a population in which each cell expressed
284 a single mutant *MSH2* variant. Sequencing of integrated libraries from genomic DNA confirmed that nearly
285 all single-codon mutations were present (97.3%) with highly uniform representation (Figure S7).

286 Sequencing errors were modeled empirically by deeply sequencing a wild-type *MSH2* plasmid, and used
287 to correct error-prone positions (Figure S9).
288
289 Each *MSH2* mutant cell pool was then selected *en masse* for MMR deficiency. To allow comparison
290 across pools, each was spiked with barcoded control cells (KO+WT: 10% of cells; KO+A636P: 0.5%).
291 Pools were then grown under selective (6-TG+blasticidin) or mock (blasticidin only) conditions for two
292 passages (Figure S6). Barc-seq of the integrated *MSH2* cDNAs confirmed that, as expected, the spiked-
293 in *MSH2* A636P cells were consistently enriched over WT by 6-TG selection (median fold-change relative
294 to mock treatment: 105; Figure S5).
295
296 To track the functional status of each *MSH2* variant, we performed amplicon sequencing of each tile
297 throughout the course of selection. Loss-of-function (LOF) scores for each variant were calculated as the
298 $\log_2$-ratio of that variant's frequency after 6-TG treatment divided by its frequency after mock treatment,
299 such that deleterious variants should score positively and neutral variants negatively (Figure 1C). LOF
300 scores strongly correlated across replicate 6-TG selections (mean pairwise Pearson's r=0.77, Figure S10).
301 As expected, mock treatment had little effect upon most variants' frequencies, except for truncating
302 variants which terminate translation before the downstream blasticidin resistance marker and were
303 therefore depleted (Figure S11).
304
305 The resulting functional effect map was substantially complete, covering 94.4% of possible *MSH2*
306 single-codon substitutions (Figure 2). Missense variant scores were bimodal, with the large majority
307 (89.4%) scoring negatively, suggesting a high degree of tolerance to single amino acid substitution (Figure
308 2G). Indeed, for over half of MSH2 residues (510/934), substitution to any other amino acid was tolerated.
309 As expected, synonymous variants predominantly scored negatively (820/841, 97.5%), with exceptions
310 likely caused by loss of function from an additional, non-programmed mutation outside the sequenced tile.
311 Most of the scored missense variants were represented by multiple equivalent codons (on average, 3.0),
312 and summarizing these internal replicates into a single, amino-acid level LOF score resulted in an overall

313 false discovery rate of 0.95%. To verify these results were generalizable across cell types, we repeated
314 the screen for two tiles (tile 14 and 15) in another MMR-proficient human cell line, HEK293, with largely
315 concordant results (Figure S12).
316
317 **Pooled Measurements Recapitulate Existing Variant Interpretations**
318
319 We sought to validate these pooled measurements by comparison to traditional, low-throughput
320 functional studies. We collated a set of 184 *MSH2* missense variants previously characterized as
321 functionally deleterious or neutral by individual cell-based[15,19,44,47–51] and/or biochemical assays[52,53],
322 discarding four variants where multiple studies disagreed and eight predicted to impact splicing, an effect
323 not measured by this approach (SpliceAI[31] score>0.2; Tables S4-5). Our LOF scores agreed with these
324 earlier reports for the great majority of variants covered (158/165, 95.8%; Figure 3A). We examined the
325 variants at which our results and previous reports disagreed, and noted that for four of those seven, our
326 LOF scores were internally consistent across multiple codons encoding the same amino acid substitution
327 (Figure S13). These may reflect false negatives or positives on the part of the previous screens, or
328 differences between this human cell model and previous yeast or *in vitro* assays.
329
330 To assess the suitability of these scores for classifying variant pathogenicity, we intersected them with
331 clinical variant databases. We retrieved all *MSH2* missense variants with consensus annotations from
332 InSight[9] or expert review in ClinVar, totaling 75 variants. After excluding nine variants predicted by SpliceAI
333 or annotated in ClinVar as splice-disruptive, our LOF scores agreed with clinical annotations for 63 of the
334 66 remaining variants (95.5%, Figure 3B). These data provide evidence to facilitate interpretation of the
335 1,374 variants without classification (i.e., VUS) or with conflicting reports. Our scores predicted that 112 of
336 these (8.2%) unresolved variants are functionally deleterious, similar to the overall rate of LOF among all
337 missense variants reachable by a single nucleotide change (7.7%; P=0.51, two-sided binomial test). This
338 result highlights the pervasiveness of benign missense variation in clinical databases and identifies a
339 subset of variants likely to be causal for Lynch Syndrome.

340

341 We next examined how these function scores varied in apparently healthy populations (Figure 3C-D).
342 The gnomAD database[23] lists 744 of the scored *MSH2* missense variants, nearly all rare (742/744 with
343 minor allele frequency < 0.5%). Among these, only 18 scored as deleterious in our assay (all singletons or
344 doubletons except the founder allele A636P), a significant depletion (P=6.9x10^{-7}, two-sided binomial test)
345 relative to randomly drawn, size-matched sets of single-base missense variants. All 14 *MSH2* missense
346 variants observed in the homozygous state in gnomAD scored as functionally neutral, as expected given
347 that biallelic MMR loss causes pediatric-onset cancer syndromes. These results reflect survivorship bias
348 which depletes adult cohorts of deleterious variants in genes underlying disorders such as Lynch
349 Syndrome, as previously noted for *MSH2* deletions[22].

350

351 **Loss of Function Scores Outperform Bioinformatic Predictors**

352

353 Bioinformatic tools are frequently used to interpret clinical variants when other forms of evidence, such
354 as co-segregation with disease, functional studies, or population variant allele frequency, are unavailable
355 or uninformative[54]. We compared the classification performance of our LOF scores with that of six
356 computational predictors, including three specific to MMR genes: MAPP-MMR[55], FoldX[56] thermostability
357 predictions from Nielsen et al[38] and PON-MMR[57], and three general-purpose tools REVEL[35], CADD[58], and
358 PolyPhen2[34]. As a truth set, we used the missense variants with previously reported functional evidence
359 (Figure 3A). LOF scores outperformed all bioinformatic classifiers in recapitulating these functional
360 classifications, reaching an area under the precision recall curve (auPR, Figure 4A) of 0.990, which
361 exceeded the six algorithms' (auPR range: 0.682-0.921). MMR-specific classifiers performed markedly
362 better (auPR mean: 0.867) than general-purpose, pathway agnostic methods (auPR mean: 0.741), which
363 displayed poor specificity, possibly reflecting the challenge of distinguishing functional effects between
364 variants in highly conserved genes such as *MSH2.*

365

366 We also tested performance of the experimental and bioinformatic scores using a fixed cutoff selected
367 for each, as would be required in practice. For LOF scores, a score cutoff of 0 was selected *a priori*, taking
368 as deleterious any variants enriched by 6-TG. For each bioinformatic algorithm, we selected a cutoff
369 (Figure S14A-B) which maximized the Matthews Correlation Coefficient (MCC), a balanced measure of
370 specificity and sensitivity[59], across the full validation set. These were broadly similar to cutoffs used
371 previously; for instance, by an earlier estimate[60], the CADD score cutoff of 24.17 used here corresponds
372 to a 96.0% probability of being an Insight Class 5 (pathogenic) variant. Using these cutoffs, LOF scores
373 reached an MCC of 0.92, higher than all six tools' (range: 0.50-0.74; Figure S14A). Notably, because
374 optimizing a cutoff score for each tool using the full validation set amounts to training and testing on the
375 same data, this comparison may overestimate their performance relative to a test on newly seen alleles,
376 whereas the LOF scores should have no such bias.
377
378 Although the bioinformatic predictions were modestly correlated with our experimental measurements
379 for variants in the functional validation set, they were markedly less concordant for other variants at those
380 same residues, or throughout *MSH2* at large (Figure 4B). Similarly weak overall agreement has also been
381 observed when benchmarking bioinformatic classifiers with deep mutational scans of other genes[61–63]. As
382 variant effect predictors are often trained on the limited number of known variants with available
383 classifications, their divergence with our experimental measurements may reflect overfitting, further
384 suggesting that the comparison to a small set of functionally characterized alleles overestimates
385 bioinformatic predictors' performance.
386
387 **Functional Constraint Highlights Structural Features**
388
389 Deep mutational scans can inform protein structure-function relationships[64,65]. On aggregate,
390 chemically conservative substitutions across MSH2 were rarely deleterious (5.63%), compared to
391 substitutions replacing hydrophobic residues with charged ones (28.0%; Figure S15). Mapping function
392 scores onto the crystal structure[39] (Figure 5A), we noted several regions of mutational intolerance

393 corresponding to structural features. The phosphate-binding Walker A motif (residues 674-676) is required
394 for the essential ATPase activity of MSH2[66] and was almost completely intolerant to mutation (50/55
395 mutations LOF, Figure 5B,C). We also noticed strong constraint at glycine 126, possibly reflecting the
396 requirement for flexibility to accommodate conformational shifts between the mismatch binding and
397 connector domains (Figure 5C)[39]. The connector domain's hydrophobic core, comprising three beta sheets
398 and inward-facing residues of the surrounding helices, was also largely functionally intolerant to
399 substitutions. Conversely, despite its name, the N-terminal mismatch binding domain (residues 1-124) was
400 largely devoid of missense LOF variants, consistent with its dispensability in yeast[67], and observations that
401 *MSH2* start codon loss is not strongly pathogenic in humans[68,69]. By contrast, prokaryotic mutS
402 homodimerizes, with both N termini making extensive DNA contacts essential for mismatch recognition[70].
403 Several positively charged clamp domain residues (K512, R524, K546), which interact with the DNA
404 backbone by hydrogen bonding[39], were strongly intolerant to substitution, especially to negatively charged
405 residues. Although computational predictions of protein stability[38] showed modest overall correlation with
406 LOF scores (Pearson's r=0.39, Figure S14), we noted a few exceptions including the ATPase Walker
407 motifs, which showed strong constraint in our data but were not predicted to be destabilizing (Figure S15),
408 suggesting mechanisms other than protein instability.
409
410 We also examined the scores of variants accepted by evolution. Given the strong pressure to maintain
411 genome integrity, *MSH2* variants rising to fixation in extant lineages are expected to be functionally neutral,
412 except for potential epistatic effects of other mutations *in cis* or *trans*[71]. We aligned the human MSH2
413 protein sequence with seven orthologs distributed across eukaryota, identifying 1,707 amino acid
414 substitutions relative to the human sequence. Of those scored, nearly all (1,627/1,639, 99.3%) had
415 negative LOF scores (Figure S16), indicating these substitutions are functionally neutral in the context of
416 the human MSH2 sequence, and supporting these scores' specificity.
417
418 **Discussion**
419

420 The mismatch repair factors underlying Lynch Syndrome are among the most intensively screened
421 genes in clinical practice, and there is an acute need for functional evidence to assist in their variants'
422 interpretation as the scope of genetic testing broadens[72,73]. Massively parallel assays provide a tractable
423 means to generate such evidence[74,75]. Here, we combined deep mutational scanning[17] with an established
424 MMR assay to generate a nearly complete functional effect map of missense variants in the key Lynch
425 Syndrome gene *MSH2*.
426
427 The resulting LOF scores have high predictive accuracy, agreeing with traditional, small-scale
428 functional reports for 158 of 165 previously tested missense variants (95.8%), which meets or exceeds the
429 level of concordance among the previous functional screens of *MSH2* missense variants. To the best of
430 our knowledge, MSH2 is the largest protein (934 aa) subjected to full-length deep mutational scanning to
431 date, demonstrating that such pooled functional screens can scale to address the large space of clinically
432 relevant human genetic variation. Additionally, this approach can be readily extended for comprehensive
433 functional annotation of variants in other key Lynch Syndrome genes, *MLH1*, *PMS2*, and *MSH6.*
434
435 Our strategy exploited the direct link from molecular dysfunction - the inability to correct replicative
436 errors - to pathogenesis in Lynch Syndrome. Accordingly, these functional measurements were highly
437 consistent with expert-reviewed variant classification records from the ClinVar database and InSiGHT
438 Group[9]. For two of the three conflicting variants, the standing classifications appear to be in error (Figure
439 S13). The first, p.Glu198Gly (InSiGHT class 1: benign), was highly deleterious in our assay (LOF score:
440 3.47), a result corroborated by mutator assays in yeast[15,51] and MNNG resistance following transient
441 overexpression in human cells[49]. Additionally, all other substitutions at Glu198 appeared deleterious in our
442 screen, except for the chemically similar p.Glu198Asp. The second example is p.Pro652His (InSiGHT
443 class 4: likely pathogenic), which along with 14 of the other 15 measured substitutions at that codon,
444 appeared neutral in our data, in agreement with its activity *in vitro*[53]. Thus, in addition to assisting the
445 resolution of VUS's, functional effect maps may allow identification and correction of rare misclassifications
446 among clinical variation databases.

447

448 Overall, *MSH2* appeared quite tolerant to missense variation, with only 10.7% of assayed missense
449 variants exhibiting loss-of-function. On face, this is surprising given the high level of sequence conservation
450 among *MSH2* orthologs (e.g., ~41% protein sequence identity between human and budding yeast), and
451 given its conserved, essential role in mismatch repair. We consider it unlikely that large swaths of LOF
452 variants have gone undetected given the strong concordance with expert-reviewed clinical interpretation
453 and prior functional studies. This degree of tolerance is remarkable in the context of available deep
454 mutational scanning data from other human genes. In terms of overall constraint, the dataset closest to
455 *MSH2* is from the transcription factor *PPARG*, in which 21.5% of missense variants scored as having
456 substantial probability of being casual for lipodystrophy[76]. Most other human genes subjected to full-length
457 mutational scans thus far have shown substantially higher overall constraint: for instance, 40.5% of
458 missense variants in the pharmacogene *NUDT15* scored as damaging[62], as were 39% of variants in the
459 homocysteine metabolic factor *CBS*[77]. A recent activity-agnostic protein stability screen showed the
460 fraction of missense variants with substantially destabilizing effects to range from 25.1-43.1% across three
461 different genes[62,78]; these could be taken as a lower bound given that an unknown fraction of true LOF
462 variants may remain stable.

463

464 The bimodal distribution of LOF scores mirrors previous functional studies in which most *MSH2*
465 missense variants have appeared either substantially functionally intact or null-like, with relatively few in
466 between. An important question arising from these functional studies is whether variants with borderline
467 scores reflect experimental noise or instead have intermediate functional activity[79]. For instance, several
468 *MSH2* alleles modeled in yeast[15] exhibited minor increases in reporter gene mutation rates (2-19X relative
469 to *MSH2* WT, compared to >200X for *MSH2* null alleles), suggesting a mild MMR defect, but all of those
470 scored as functionally neutral in our data. Of the three (p.L390F, p.M688I, and p.E886G) tested in other
471 studies, all appeared functionally neutral, corroborating our results and suggesting either a greater
472 sensitivity to functional defects in the yeast model or potentially some functional divergence between the
473 orthologs[16]. Other variants have conflicting evidence which will require additional studies to resolve, for

474 instance p.L93F, which showed intermediate activity (~51%) in a cell-free MMR assay[53], was undetected
475 in a mouse ES cell based clonogenic screen for pathogenic alleles[19] and was marginally neutral in our data
476 (LOF score: -0.26).
477
478 For any such alleles that do behave as hypomorphs in functional assays, it remains unclear whether
479 these meaningfully contribute to Lynch Syndrome risk[51,80]. Complicating this question is the challenge of
480 establishing a truth set of moderate-risk *MSH2* variants in family or case-control studies, as with further
481 reduced penetrance and later age of cancer onset, these may resemble common sporadic cancers.
482 However, anecdotes suggest that even severely hypomorphic alleles of MMR factors may retain enough
483 activity to set them apart from complete LOF alleles. For instance, a splice-disruptive mutation which
484 reduces PMS2 expression by >10-fold retains enough activity that when homozygous, it results in a form
485 of constitutional MMR deficiency which is highly attenuated, with later onset and less profound
486 microsatellite instability compared to truly null biallelic mutations[81]. As increasingly large variation datasets
487 coupled to electronic health records become available[82–84], it may become possible to examine whether
488 variants with intermediate functional scores, on aggregate, confer increased Lynch Syndrome risk, and
489 whether individuals carrying one of these alleles opposite a *bona fide* pathogenic allele present with
490 biallelic MMR deficiency.
491
492 One limitation of these cDNA-based measurements is that they cannot model effects upon splicing,
493 although among known Lynch Syndrome variants and in saturation screens of other hereditary cancer
494 syndrome genes[85], splice disruption accounts for only a small fraction of pathogenic variants. In the future,
495 splicing effects could be accounted for by incorporating improved bioinformatic predictions[31] or multiplexed
496 assays[86–88]. Another potential limitation is that our *MSH2* LOF scores are not a direct measure of mutation
497 rates associated with each variant, to the extent that these could differ across *MSH2* variants. We instead
498 used a close proxy for MMR dysfunction, treatment with the purine analog 6-TG, which selectively enrichies
499 for MMR-defective cells which lack the ability to remove the resulting lesions. As with other deep mutational

500 scans, these results may be further refined with orthogonal functional selections[62,89] or complemented by
501 specialized assays for protein stability[78], localization[90], or partner (MSH6) binding.
502
503 We demonstrate that massively parallel functional assays can accurately measure the impacts of
504 variants in the key Lynch Syndrome gene *MSH2*. This functional effect map, if rationally combined[54,91] with
505 other lines of clinical evidence[9], will enable more accurate classification of Lynch Syndrome variants.
506 Adding confidence and accuracy to Lynch Syndrome variant interpretation will afford carriers of pathogenic
507 variants the benefits of potentially life-saving early detection and medical interventions[92].

508 **Supplemental Data**

509 Supplemental Data include sixteen figures and five tables

510 **Acknowledgements**

511 We thank M. Meisler, A. Antonellis, E. Stoffel, S. Hemker, and A. Glazer for helpful discussions, J. Moran
512 for providing sequencer access, and J. Moldovan for assistance with clonogenic assays. This work was
513 supported by the National Institute of General Medical Sciences (5R01GM129123 to J.O.K.) and a
514 Precision Health Fellowship from the University of Michigan (to X.J.).

515 **Declaration of Interests**

516 The authors declare no competing interests.

References

1. Lynch, H.T., and Krush, A.J. (1971). Cancer family “G” revisited: 1895-1970. Cancer *27*, 1505–1511.

2. Leach, F.S., Nicolaides, N.C., Papadopoulos, N., Liu, B., Jen, J., Parsons, R., Peltomäki, P., Sistonen, P., Aaltonen, L.A., and Nyström-Lahti, M. (1993). Mutations of a mutS homolog in hereditary nonpolyposis colorectal cancer. Cell *75*, 1215–1225.

3. Fishel, R., Lescoe, M.K., Rao, M.R., Copeland, N.G., Jenkins, N.A., Garber, J., Kane, M., and Kolodner, R. (1994). The human mutator gene homolog MSH2 and its association with hereditary nonpolyposis colon cancer. Cell *77*, 1 p following 166.

4. Bronner, C.E., Baker, S.M., Morrison, P.T., Warren, G., Smith, L.G., Lescoe, M.K., Kane, M., Earabino, C., Lipford, J., Lindblom, A., et al. (1994). Mutation in the DNA mismatch repair gene

homologue hMLH 1 is associated with hereditary non-polyposis colon cancer. Nature *368*, 258–261.

5. Papadopoulos, N., Nicolaides, N.C., Wei, Y.F., Ruben, S.M., Carter, K.C., Rosen, C.A., Haseltine, W.A., Fleischmann, R.D., Fraser, C.M., and Adams, M.D. (1994). Mutation of a mutL homolog in hereditary colon cancer. Science *263*, 1625–1629.

6. Win, A.K., Jenkins, M.A., Dowty, J.G., Antoniou, A.C., Lee, A., Giles, G.G., Buchanan, D.D., Clendenning, M., Rosty, C., Ahnen, D.J., et al. (2017). Prevalence and Penetrance of Major Genes and Polygenes for Colorectal Cancer. Cancer Epidemiol. Biomarkers Prev. *26*, 404–412.

7. Haraldsdottir, S., Rafnar, T., Frankel, W.L., Einarsdottir, S., Sigurdsson, A., Hampel, H., Snaebjornsson, P., Masson, G., Weng, D., Arngrimsson, R., et al. (2017). Comprehensive population-wide analysis of Lynch syndrome in Iceland reveals founder mutations in MSH6 and PMS2. Nat. Commun. *8*, 14755.

8. Kalia, S.S., Adelman, K., Bale, S.J., Chung, W.K., Eng, C., Evans, J.P., Herman, G.E., Hufnagel, S.B., Klein, T.E., Korf, B.R., et al. (2017). Recommendations for reporting of secondary findings in clinical exome and genome sequencing, 2016 update (ACMG SF v2. 0): a policy statement of the American College of Medical Genetics and Genomics. Genet. Med. *19*, 249.

9. Thompson, B.A., Spurdle, A.B., Plazzer, J.-P., Greenblatt, M.S., Akagi, K., Al-Mulla, F., Bapat, B., Bernstein, I., Capellá, G., den Dunnen, J.T., et al. (2014). Application of a 5-tiered scheme for standardized classification of 2,360 unique mismatch repair gene variants in the InSiGHT locus-specific database. Nat. Genet. *46*, 107–115.

10. Giardiello, F.M., Allen, J.I., Axilbund, J.E., Boland, C.R., Burke, C.A., Burt, R.W., Church, J.M., Dominitz, J.A., Johnson, D.A., Kaltenbach, T., et al. (2014). Guidelines on genetic evaluation and management of Lynch syndrome: a consensus statement by the US Multi-Society Task Force on Colorectal Cancer. Dis. Colon Rectum *57*, 1025–1048.

11. Møller, P., Seppälä, T.T., Bernstein, I., Holinski-Feder, E., Sala, P., Gareth Evans, D., Lindblom, A., Macrae, F., Blanco, I., Sijmons, R.H., et al. (2018). Cancer risk and survival in path_MMR carriers by gene and gender up to 75 years of age: a report from the Prospective Lynch Syndrome Database. Gut *67*, 1306–1316.

12. Brnich, S.E., Rivera-Muñoz, E.A., and Berg, J.S. (2018). Quantifying the potential of functional evidence to reclassify variants of uncertain significance in the categorical and Bayesian interpretation frameworks. Hum. Mutat. *39*, 1531–1541.

13. Richards, S., Aziz, N., Bale, S., Bick, D., Das, S., Gastier-Foster, J., Grody, W.W., Hegde, M., Lyon, E., Spector, E., et al. (2015). Standards and guidelines for the interpretation of sequence variants: a joint consensus recommendation of the American College of Medical Genetics and Genomics and the Association for Molecular Pathology. Genet. Med. *17*, 405–424.

14. Clark, A.B., Cook, M.E., Tran, H.T., Gordenin, D.A., Resnick, M.A., and Kunkel, T.A. (1999). Functional analysis of human MutSα and MutSβ complexes in yeast. Nucleic Acids Res. *27*, 736–742.

15. Gammie, A.E., Erdeniz, N., Beaver, J., Devlin, B., Nanji, A., and Rose, M.D. (2007). Functional characterization of pathogenic human MSH2 missense mutations in Saccharomyces cerevisiae. Genetics *177*, 707–721.

16. Shimodaira, H., Filosi, N., Shibata, H., Suzuki, T., Radice, P., Kanamaru, R., Friend, S.H., Kolodner, R.D., and Ishioka, C. (1998). Functional analysis of human MLH1 mutations in Saccharomyces cerevisiae. Nat. Genet. *19*, 384–389.

17. Fowler, D.M., and Fields, S. (2014). Deep mutational scanning: a new style of protein science. Nat.

Methods *11*, 801–807.

18. Swann, P.F., Waters, T.R., Moulton, D.C., Xu, Y.Z., Zheng, Q., Edwards, M., and Mace, R. (1996). Role of postreplicative DNA mismatch repair in the cytotoxic action of thioguanine. Science *273*, 1109–1111.

19. Houlleberghs, H., Dekker, M., Lantermans, H., Kleinendorst, R., Dubbink, H.J., Hofstra, R.M.W., Verhoef, S., and Te Riele, H. (2016). Oligonucleotide-directed mutagenesis screen to identify pathogenic Lynch syndrome-associated MSH2 DNA mismatch repair gene variants. Proc. Natl. Acad. Sci. U. S. A. *113*, 4128–4133.

20. Yan, T., Berry, S.E., Desai, A.B., and Kinsella, T.J. (2003). DNA mismatch repair (MMR) mediates 6-thioguanine genotoxicity by introducing single-strand breaks to signal a G2-M arrest in MMR-proficient RKO cells. Clin. Cancer Res. *9*, 2327–2334.

21. Mojas, N., Lopes, M., and Jiricny, J. (2007). Mismatch repair-dependent processing of methylation damage gives rise to persistent single-stranded gaps in newly replicated DNA. Genes Dev. *21*, 3342–3355.

22. Aguirre, M., Rivas, M.A., and Priest, J. (2019). Phenome-wide Burden of Copy-Number Variation in the UK Biobank. Am. J. Hum. Genet. *105*, 373–383.

23. Karczewski, K.J., Francioli, L.C., Tiao, G., Cummings, B.B., Alföldi, J., Wang, Q., Collins, R.L., Laricchia, K.M., Ganna, A., Birnbaum, D.P., et al. (2020). The mutational constraint spectrum quantified from variation in 141,456 humans. Nature *581*, 434–443.

24. Ran, F.A., Hsu, P.D., Wright, J., Agarwala, V., Scott, D.A., and Zhang, F. (2013). Genome engineering using the CRISPR-Cas9 system. Nat. Protoc. *8*, 2281–2308.

25. Kitzman, J.O., Starita, L.M., Lo, R.S., Fields, S., and Shendure, J. (2015). Massively parallel single-amino-acid mutagenesis. Nat. Methods *12*, 203–206, 4 p following 206.

26. Rohland, N., and Reich, D. (2012). Cost-effective, high-throughput DNA sequencing libraries for multiplexed target capture. Genome Res. *22*, 939–946.

27. Picelli, S., Björklund, A.K., Reinius, B., Sagasser, S., Winberg, G., and Sandberg, R. (2014). Tn5 transposase and tagmentation procedures for massively scaled sequencing projects. Genome Res. *24*, 2033–2040.

28. Joung, J., Konermann, S., Gootenberg, J.S., Abudayyeh, O.O., Platt, R.J., Brigham, M.D., Sanjana, N.E., and Zhang, F. (2017). Genome-scale CRISPR-Cas9 knockout and transcriptional activation screening. Nat. Protoc. *12*, 828–863.

29. Zhang, J., Kobert, K., Flouri, T., and Stamatakis, A. (2014). PEAR: a fast and accurate Illumina Paired-End reAd mergeR. Bioinformatics *30*, 614–620.

30. Zorita, E., Cuscó, P., and Filion, G.J. (2015). Starcode: sequence clustering based on all-pairs search. Bioinformatics *31*, 1913–1919.

31. Jaganathan, K., Kyriazopoulou Panagiotopoulou, S., McRae, J.F., Darbandi, S.F., Knowles, D., Li, Y.I., Kosmicki, J.A., Arbelaez, J., Cui, W., Schwartz, G.B., et al. (2019). Predicting Splicing from Primary Sequence with Deep Learning. Cell *176*, 535–548.e24.

32. Carlson, J., Locke, A.E., Flickinger, M., Zawistowski, M., Levy, S., Myers, R.M., Boehnke, M., Kang, H.M., Scott, L.J., Li, J.Z., et al. (2018). Extremely rare variants reveal patterns of germline mutation rate heterogeneity in humans. Nat. Commun. *9*, 3753.

33. Rentzsch, P., Witten, D., Cooper, G.M., Shendure, J., and Kircher, M. (2019). CADD: predicting the deleteriousness of variants throughout the human genome. Nucleic Acids Res. *47*, D886–D894.

34. Adzhubei, I.A., Schmidt, S., Peshkin, L., Ramensky, V.E., Gerasimova, A., Bork, P., Kondrashov, A.S., and Sunyaev, S.R. (2010). A method and server for predicting damaging missense mutations. Nat. Methods *7*, 248–249.

35. Ioannidis, N.M., Rothstein, J.H., Pejaver, V., Middha, S., McDonnell, S.K., Baheti, S., Musolf, A., Li, Q., Holzinger, E., Karyadi, D., et al. (2016). REVEL: An Ensemble Method for Predicting the Pathogenicity of Rare Missense Variants. Am. J. Hum. Genet. *99*, 877–885.

36. Ali, H., Olatubosun, A., and Vihinen, M. (2012). Classification of mismatch repair gene missense variants with PON-MMR. Hum. Mutat. *33*, 642–650.

37. Chao, E., Velasquez, J., Witherspoon, M., Rozek, L., Ng, P., Gruber, S., Watson, P., Rennert, G., Anton-Culver, H., Lynch, H., et al. (2008). Accurate classification of missense variants in MLH1/MSH2 with MAPP-MMR. Cancer Res. *68*, LB – 14 – LB – 14.

38. Nielsen, S.V., Stein, A., Dinitzen, A.B., Papaleo, E., Tatham, M.H., Poulsen, E.G., Kassem, M.M., Rasmussen, L.J., Lindorff-Larsen, K., and Hartmann-Petersen, R. (2017). Predicting the impact of Lynch syndrome-causing missense mutations from structural calculations. PLoS Genet. *13*, e1006739.

39. Warren, J.J., Pohlhaus, T.J., Changela, A., Iyer, R.R., Modrich, P.L., and Beese, L.S. (2007). Structure of the Human MutSα DNA Lesion Recognition Complex. Mol. Cell *26*, 579–592.

40. Touw, W.G., Baakman, C., Black, J., te Beek, T.A.H., Krieger, E., Joosten, R.P., and Vriend, G. (2015). A series of PDB-related databanks for everyday needs. Nucleic Acids Research *43*, D364–D368.

41. Edgar, R.C. (2004). MUSCLE: multiple sequence alignment with high accuracy and high throughput. Nucleic Acids Res. *32*, 1792–1797.

42. Harmsen, T., Klaasen, S., van de Vrugt, H., and Te Riele, H. (2018). DNA mismatch repair and oligonucleotide end-protection promote base-pair substitution distal from a CRISPR/Cas9-induced DNA break. Nucleic Acids Res. *46*, 2945–2955.

43. Foulkes, W.D., Thiffault, I., Gruber, S.B., Horwitz, M., Hamel, N., Lee, C., Shia, J., Markowitz, A., Figer, A., Friedman, E., et al. (2002). The Founder Mutation MSH2*1906G→C Is an Important Cause of Hereditary Nonpolyposis Colorectal Cancer in the Ashkenazi Jewish Population. Am. J. Hum. Genet. *71*, 1395–1412.

44. Wielders, E.A.L., Hettinger, J., Dekker, R., Kets, C.M., Ligtenberg, M.J., Mensenkamp, A.R., van den Ouweland, A.M.W., Prins, J., Wagner, A., Dinjens, W.N.M., et al. (2014). Functional analysis of MSH2 unclassified variants found in suspected Lynch syndrome patients reveals pathogenicity due to attenuated mismatch repair. J. Med. Genet. *51*, 245–253.

45. Weile, J., Sun, S., Cote, A.G., Knapp, J., Verby, M., Mellor, J.C., Wu, Y., Pons, C., Wong, C., van Lieshout, N., et al. (2017). A framework for exhaustively mapping functional missense variants. Mol. Syst. Biol. *13*, 957.

46. Sack, L.M., Davoli, T., Xu, Q., Li, M.Z., and Elledge, S.J. (2016). Sources of Error in Mammalian Genetic Screens. G3 *6*, 2781–2790.

47. Rath, A., Mishra, A., Ferreira, V.D., Hu, C., Omerza, G., Kelly, K., Hesse, A., Reddi, H.V., Grady, J.P., and Heinen, C.D. (2019). Functional interrogation of Lynch syndrome-associated MSH2 missense variants via CRISPR-Cas9 gene editing in human embryonic stem cells. Hum. Mutat. *40*, 2044–2056.

48. Mastrocola, A.S., and Heinen, C.D. (2010). Lynch syndrome-associated mutations in MSH2 alter DNA repair and checkpoint response functions in vivo. Hum. Mutat. *31*, E1699–E1708.

49. Bouvet, D., Bodo, S., Munier, A., Guillerm, E., Bertrand, R., Colas, C., Duval, A., Coulet, F., and Muleris, M. (2019). Methylation Tolerance-Based Functional Assay to Assess Variants of Unknown Significance in the MLH1 and MSH2 Genes and Identify Patients With Lynch Syndrome. Gastroenterology *157*, 421–431.

50. Drost, M., Lützen, A., van Hees, S., Ferreira, D., Calléja, F., Zonneveld, J.B.M., Nielsen, F.C., Rasmussen, L.J., and de Wind, N. (2013). Genetic screens to identify pathogenic gene variants in the common cancer predisposition Lynch syndrome. Proc. Natl. Acad. Sci. U. S. A. *110*, 9403–9408.

51. Martinez, S.L., and Kolodner, R.D. (2010). Functional analysis of human mismatch repair gene mutations identifies weak alleles and polymorphisms capable of polygenic interactions. Proc. Natl. Acad. Sci. U. S. A. *107*, 5070–5075.

52. Drost, M., Zonneveld, J.B.M., van Hees, S., Rasmussen, L.J., Hofstra, R.M.W., and de Wind, N. (2012). A rapid and cell-free assay to test the activity of lynch syndrome-associated MSH2 and MSH6 missense variants. Human Mutation *33*, 488–494.

53. Drost, M., Tiersma, Y., Thompson, B.A., Frederiksen, J.H., Keijzers, G., Glubb, D., Kathe, S., Osinga, J., Westers, H., Pappas, L., et al. (2019). A functional assay–based procedure to classify mismatch repair gene variants in Lynch syndrome. Genet. Med. *21*, 1486–1496.

54. Brnich, S.E., Abou Tayoun, A.N., Couch, F.J., Cutting, G.R., Greenblatt, M.S., Heinen, C.D., Kanavy, D.M., Luo, X., McNulty, S.M., Starita, L.M., et al. (2019). Recommendations for application of the functional evidence PS3/BS3 criterion using the ACMG/AMP sequence variant interpretation framework. Genome Med. *12*, 3.

55. Chao, E.C., Velasquez, J.L., Witherspoon, M.S.L., Rozek, L.S., Peel, D., Ng, P., Gruber, S.B., Watson, P., Rennert, G., Anton-Culver, H., et al. (2008). Accurate classification of MLH1/MSH2 missense variants with multivariate analysis of protein polymorphisms-mismatch repair (MAPP-MMR). Hum. Mutat. *29*, 852–860.

56. Schymkowitz, J., Borg, J., Stricher, F., Nys, R., Rousseau, F., and Serrano, L. (2005). The FoldX web server: an online force field. Nucleic Acids Res. *33*, W382–W388.

57. Ali, H., Olatubosun, A., and Vihinen, M. (2012). Classification of mismatch repair gene missense variants with PON-MMR. Hum. Mutat. *33*, 642–650.

58. Kircher, M., Witten, D.M., Jain, P., O'Roak, B.J., Cooper, G.M., and Shendure, J. (2014). A general framework for estimating the relative pathogenicity of human genetic variants. Nat. Genet. *46*, 310–315.

59. Chicco, D., and Jurman, G. (2020). The advantages of the Matthews correlation coefficient (MCC) over F1 score and accuracy in binary classification evaluation. BMC Genomics *21*, 6.

60. van der Velde, K.J., Kuiper, J., Thompson, B.A., Plazzer, J.-P., van Valkenhoef, G., de Haan, M., Jongbloed, J.D.H., Wijmenga, C., de Koning, T.J., Abbott, K.M., et al. (2015). Evaluation of CADD Scores in Curated Mismatch Repair Gene Variants Yields a Model for Clinical Validation and Prioritization. Hum. Mutat. *36*, 712–719.

61. Li, J., Zhao, T., Zhang, Y., Zhang, K., Shi, L., Chen, Y., Wang, X., and Sun, Z. (2018). Performance evaluation of pathogenicity-computation methods for missense variants. Nucleic Acids Res. *46*, 7793–7804.

62. Suiter, C.C., Moriyama, T., Matreyek, K.A., Yang, W., Scaletti, E.R., Nishii, R., Yang, W., Hoshitsuki,

K., Singh, M., Trehan, A., et al. (2020). Massively parallel variant characterization identifies NUDT15 alleles associated with thiopurine toxicity. Proc. Natl. Acad. Sci. U. S. A.

63. Livesey, B.J., and Marsh, J.A. (2020). Using deep mutational scanning to benchmark variant effect predictors and identify disease mutations. Mol. Syst. Biol. *16*, e9380.

64. Gray, V.E., Hause, R.J., and Fowler, D.M. (2017). Analysis of Large-Scale Mutagenesis Data To Assess the Impact of Single Amino Acid Substitutions. Genetics *207*, 53–61.

65. Rollins, N.J., Brock, K.P., Poelwijk, F.J., Stiffler, M.A., Gauthier, N.P., Sander, C., and Marks, D.S. (2019). Inferring protein 3D structure from deep mutation scans. Nat. Genet. *51*, 1170–1176.

66. Graham, W.J., Putnam, C.D., and Kolodner, R.D. (2018). The properties of Msh2–Msh6 ATP binding mutants suggest a signal amplification mechanism in DNA mismatch repair. J. Biol. Chem.

67. Kumar, C., Piacente, S.C., Sibert, J., Bukata, A.R., O'Connor, J., Alani, E., and Surtees, J.A. (2011). Multiple Factors Insulate Msh2–Msh6 Mismatch Repair Activity from Defects in Msh2 Domain I. J. Mol. Biol. *411*, 765–780.

68. Cyr, J.L., Brown, G.D., Stroop, J., and Heinen, C.D. (2012). The predicted truncation from a cancer-associated variant of the MSH2 initiation codon alters activity of the MSH2-MSH6 mismatch repair complex. Molecular Carcinogenesis *51*, 647–658.

69. Kets, C.M., Hoogerbrugge, N., van Krieken, J.H.J.M., Goossens, M., Brunner, H.G., and Ligtenberg, M.J.L. (2009). Compound heterozygosity for two MSH2 mutations suggests mild consequences of the initiation codon variant c.1A>G of MSH2. Eur. J. Hum. Genet. *17*, 159–164.

70. Obmolova, G., Ban, C., Hsieh, P., and Yang, W. (2000). Crystal structures of mismatch repair protein MutS and its complex with a substrate DNA. Nature *407*, 703–710.

71. Jordan, D.M., Frangakis, S.G., Golzio, C., Cassa, C.A., Kurtzberg, J., Task Force for Neonatal Genomics, Davis, E.E., Sunyaev, S.R., and Katsanis, N. (2015). Identification of cis-suppression of human disease mutations by comparative genomics. Nature *524*, 225–229.

72. Dinh, T.A., Rosner, B.I., Atwood, J.C., Boland, C.R., Syngal, S., Vasen, H.F.A., Gruber, S.B., and Burt, R.W. (2011). Health benefits and cost-effectiveness of primary genetic screening for Lynch syndrome in the general population. Cancer Prev. Res. *4*, 9–22.

73. King, M.-C., Levy-Lahad, E., and Lahad, A. (2014). Population-based screening for BRCA1 and BRCA2: 2014 Lasker Award. JAMA *312*, 1091–1092.

74. Starita, L.M., Ahituv, N., Dunham, M.J., Kitzman, J.O., Roth, F.P., Seelig, G., Shendure, J., and Fowler, D.M. (2017). Variant Interpretation: Functional Assays to the Rescue. Am. J. Hum. Genet. *101*, 315–325.

75. Weile, J., and Roth, F.P. (2018). Multiplexed assays of variant effects contribute to a growing genotype-phenotype atlas. Hum. Genet. *137*, 665–678.

76. Majithia, A.R., Tsuda, B., Agostini, M., Gnanapradeepan, K., Rice, R., Peloso, G., Patel, K.A., Zhang, X., Broekema, M.F., Patterson, N., et al. (2016). Prospective functional classification of all possible missense variants in PPARG. Nat. Genet. *48*, 1570–1575.

77. Sun, S., Weile, J., Verby, M., Wu, Y., Wang, Y., Cote, A.G., Fotiadou, I., Kitaygorodsky, J., Vidal, M., Rine, J., et al. (2020). A proactive genotype-to-patient-phenotype map for cystathionine beta-synthase. Genome Med. *12*, 13.

78. Matreyek, K.A., Starita, L.M., Stephany, J.J., Martin, B., Chiasson, M.A., Gray, V.E., Kircher, M., Khechaduri, A., Dines, J.N., Hause, R.J., et al. (2018). Multiplex assessment of protein variant abundance by massively parallel sequencing. Nat. Genet. *50*, 874–882.

79. Spurdle, A.B., Whiley, P.J., Thompson, B., Feng, B., Healey, S., Brown, M.A., Pettigrew, C., kConFab, Van Asperen, C.J., Ausems, M.G.E.M., et al. (2012). BRCA1 R1699Q variant displaying ambiguous functional abrogation confers intermediate breast and ovarian cancer risk. J. Med. Genet. *49*, 525–532.

80. Heinen, C.D., and Juel Rasmussen, L. (2012). Determining the functional significance of mismatch repair gene missense variants using biochemical and cellular assays. Hered. Cancer Clin. Pract. *10*, 9.

81. Li, L., Hamel, N., Baker, K., McGuffin, M.J., Couillard, M., Gologan, A., Marcus, V.A., Chodirker, B., Chudley, A., Stefanovici, C., et al. (2015). A homozygous PMS2 founder mutation with an attenuated constitutional mismatch repair deficiency phenotype. J. Med. Genet. *52*, 348–352.

82. Carey, D.J., Fetterolf, S.N., Davis, F.D., Faucett, W.A., Kirchner, H.L., Mirshahi, U., Murray, M.F., Smelser, D.T., Gerhard, G.S., and Ledbetter, D.H. (2016). The Geisinger MyCode community health initiative: an electronic health record–linked biobank for precision medicine research. Genet. Med. *18*, 906–913.

83. Bycroft, C., Freeman, C., Petkova, D., Band, G., Elliott, L.T., Sharp, K., Motyer, A., Vukcevic, D., Delaneau, O., O'Connell, J., et al. (2018). The UK Biobank resource with deep phenotyping and genomic data. Nature *562*, 203–209.

84. Grzymski, J.J., Elhanan, G., Morales Rosado, J.A., Smith, E., Schlauch, K.A., Read, R., Rowan, C., Slotnick, N., Dabe, S., Metcalf, W.J., et al. (2020). Population genetic screening efficiently identifies carriers of autosomal dominant diseases. Nat. Med.

85. Findlay, G.M., Daza, R.M., Martin, B., Zhang, M.D., Leith, A.P., Gasperini, M., Janizek, J.D., Huang, X., Starita, L.M., and Shendure, J. (2018). Accurate classification of BRCA1 variants with saturation genome editing. Nature *562*, 217–222.

86. Adamson, S.I., Zhan, L., and Graveley, B.R. (2018). Vex-seq: high-throughput identification of the impact of genetic variation on pre-mRNA splicing efficiency. Genome Biol. *19*, 71.

87. Cheung, R., Insigne, K.D., Yao, D., Burghard, C.P., Wang, J., Hsiao, Y.-H.E., Jones, E.M., Goodman, D.B., Xiao, X., and Kosuri, S. (2019). A Multiplexed Assay for Exon Recognition Reveals that an Unappreciated Fraction of Rare Genetic Variants Cause Large-Effect Splicing Disruptions. Mol. Cell *73*, 183–194.e8.

88. Soemedi, R., Cygan, K.J., Rhine, C.L., Wang, J., Bulacan, C., Yang, J., Bayrak-Toydemir, P., McDonald, J., and Fairbrother, W.G. (2017). Pathogenic variants that alter protein code often disrupt splicing. Nat. Genet. *49*, 848–855.

89. Mighell, T.L., Thacker, S., Fombonne, E., Eng, C., and O'Roak, B.J. (2020). An Integrated Deep-Mutational-Scanning Approach Provides Clinical Insights on PTEN Genotype-Phenotype Relationships. Am. J. Hum. Genet. *106*, 818–829.

90. Penn, W.D., McKee, A.G., Kuntz, C.P., Woods, H., Nash, V., Gruenhagen, T.C., Roushar, F.J., Chandak, M., Hemmerich, C., Rusch, D.B., et al. (2020). Probing biophysical sequence constraints within the transmembrane domains of rhodopsin by deep mutational scanning. Sci Adv *6*, eaay7505.

91. Tavtigian, S.V., Greenblatt, M.S., Harrison, S.M., Nussbaum, R.L., Prabhu, S.A., Boucher, K.M., Biesecker, L.G., and ClinGen Sequence Variant Interpretation Working Group (ClinGen SVI) (2018). Modeling the ACMG/AMP variant classification guidelines as a Bayesian classification framework. Genet.

Med. *20*, 1054–1060.

92. Hampel, H., and de la Chapelle, A. (2011). The search for unaffected individuals with Lynch syndrome: do the ends justify the means? Cancer Prev. Res. *4*, 1–5.

517 **Figures**

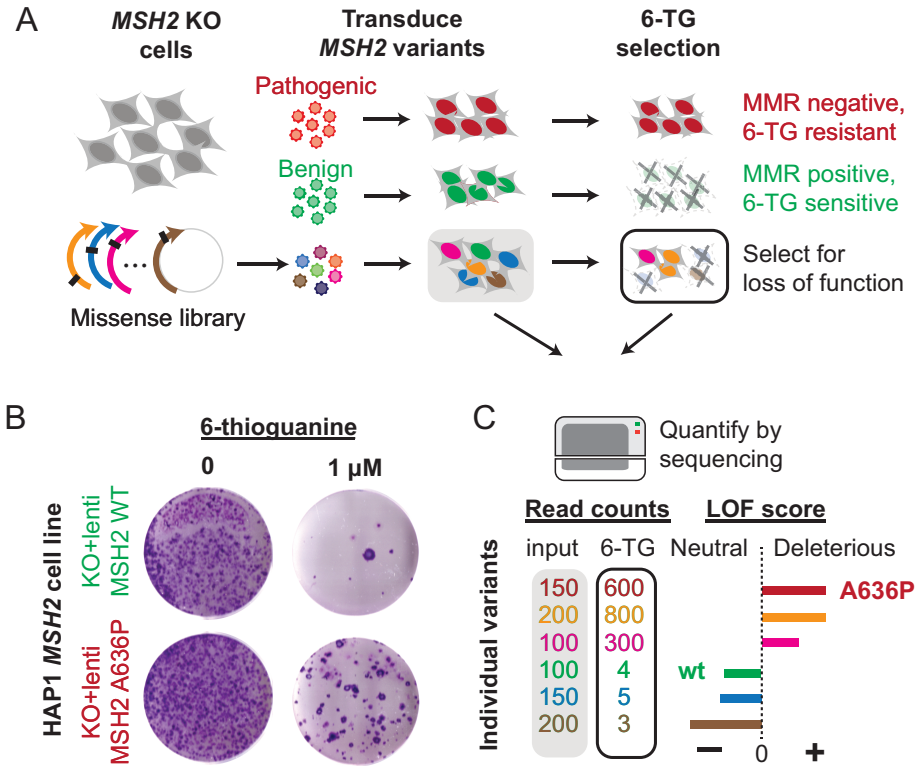

518

519 **Figure 1. Overview of *MSH2* functional screen.** (A) Generating and testing *MSH2* variant function in
520 isogenic human cells. Cells with pathogenic loss-of-function variants (top) are resistant to 6-thioguanine
521 (6-TG), while complementation by a benign functional variant (middle) restores 6-TG sensitivity. In a pooled
522 screen (bottom), a mixed library of *MSH2* missense variants is transduced, and 6-TG treatment selects for
523 loss-of-function variants. (B) 6-TG resistance reflects MMR function in human cells. HAP1 *MSH2* KO cells
524 were transduced with either functional (wild-type) *MSH2* cDNA (upper row) or loss-of-function missense
525 variant A636P (bottom row), and grown for 4 days without (left) or with 6-TG (1 uM, right). (C) Readout
526 using deep sequencing to quantify abundances of each *MSH2* allele before and after 6-TG selection. The
527 resulting loss-of-function (LOF) score is positive for deleterious variants and negative for functionally
528 neutral ones.

529

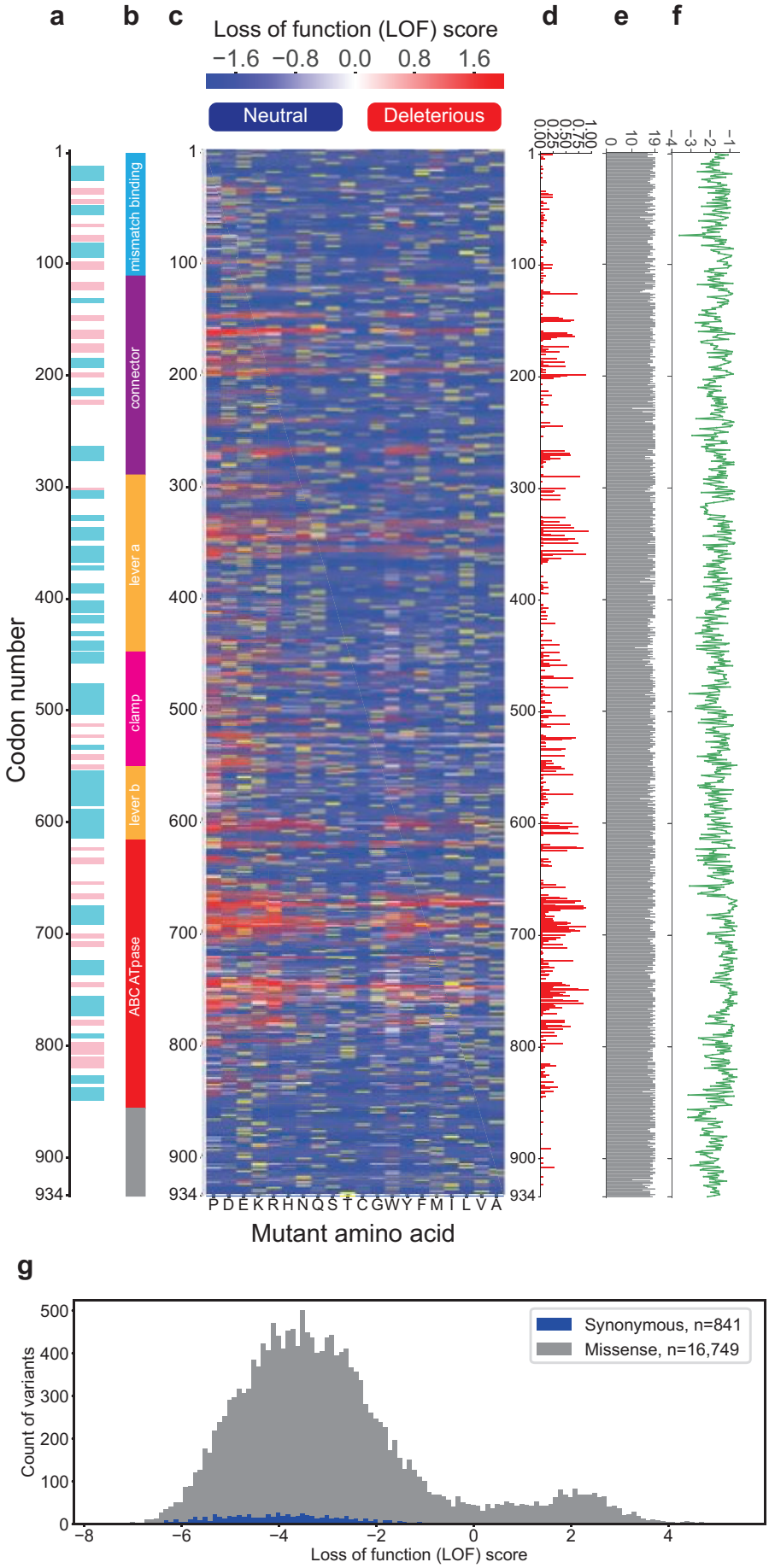
a
b
c
d
e
f
Loss of function (LOF) score
−1.6 −0.8 0.0 0.8 1.6
Neutral
Deleterious
mismatch binding
connector
lever a
clamp
lever b
ABC ATpase
Codon number
P D E K R H N Q S T C G W Y F M I L V A
Mutant amino acid
g
Synonymous, n=841
Missense, n=16,749
Count of variants
Loss of function (LOF) score

Figure 2. **Functional effect map of *MSH2* missense variants.** (A) MSH2 secondary structure (cyan: alpha helices, pink: beta sheets), and (B) protein domains. (C) Heatmap of loss-of-function (LOF) scores after mutating each of 934 residues in MSH2 (rows) to each of 19 other possible amino acids (columns). Negative scores (shaded blue) indicate functionally neutral variants, while positive scores (red) indicate deleterious ones; Yellow denotes wild-type amino acid, gray: no data. (D) Fractions of substitutions which are disruptive (LOF score>0) by position. (E) Number of scored missense variants by position (max. possible: 19). (F) Evolutionary conservation (PSIC score) by position. (G) Distributions of LOF scores, shaded by variant class.

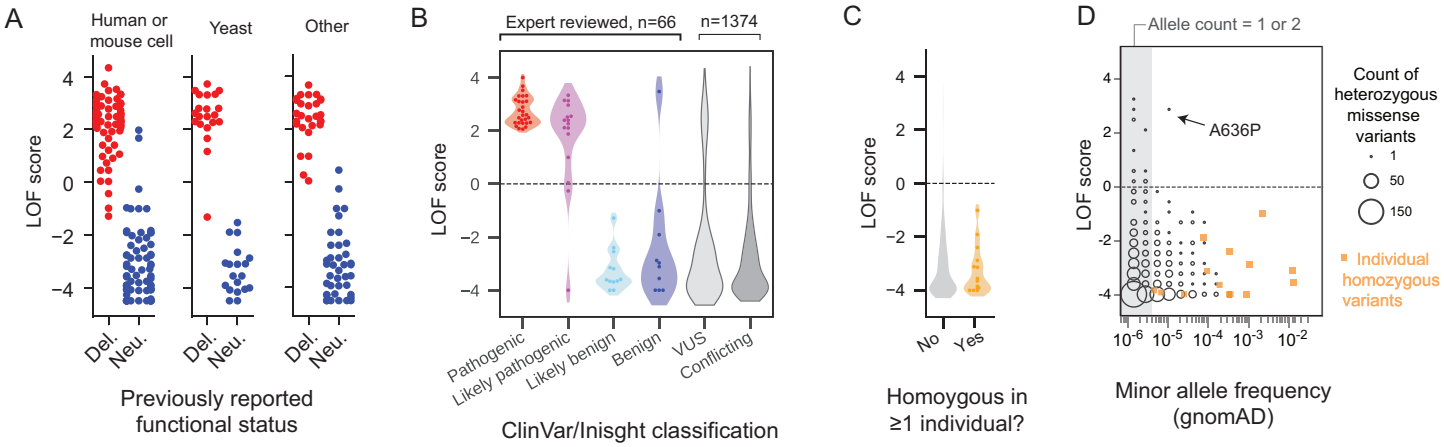

Figure 3. Concordance with existing functional and clinical classifications. (A) Measured LOF scores (y-axis) for published *MSH2* missense variants (n=295 reports covering 184 distinct variants), separated by previous characterization (x-axis) in individual cellular or biochemical assays. (B) LOF scores for patient missense variants from ClinVar and InSight databases, by variant classification. (C) Distributions of LOF scores of *MSH2* missense variants in the gnomAD database[23], for variants which do not appear in the homozygous state (gray) or those which do in ≥1 individual (orange). (D) LOF score versus gnomAD allele frequency for *MSH2* missense variants; size of circle denotes number of heterozygous variants; orange squares mark missense variants observed in homozygous state in ≥1 individual. Gray region denotes singletons/doubletons (gnomAD allele count ≤2).

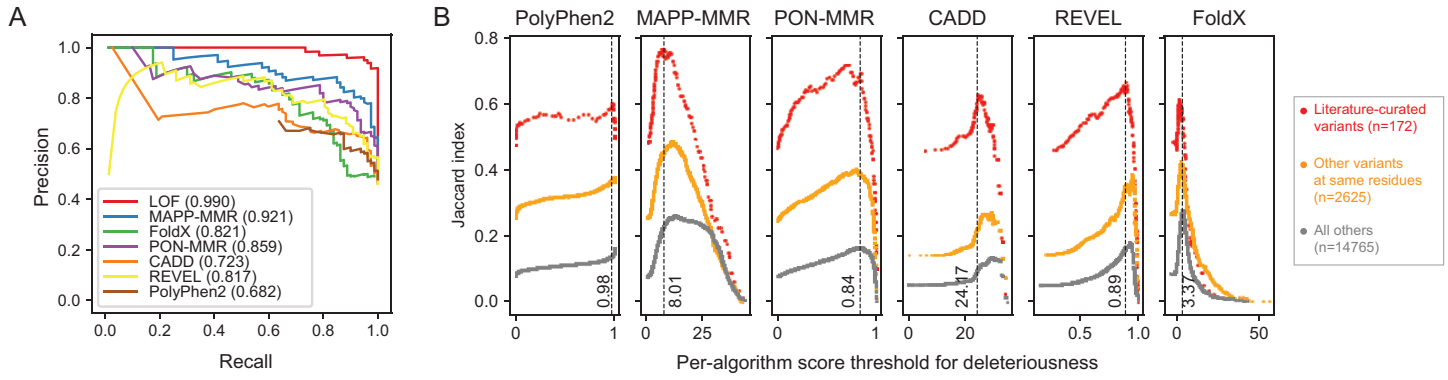

Figure 4. Comparison with bioinformatic predictions of pathogenicity (A) Precision-recall curves show LOF scores outperform all tested bioinformatic callers in predicting the functional status of the validation set of variants with known effect; area under the curve indicated for each. (B) Concordance of each bioinformatic predictor (Jaccard Index) with experimental LOF scores is plotted versus algorithm-specific score threshold for deleteriousness. Algorithms were most concordant with LOF scores among mutations with published functional data (red), followed by other mutations at the same residues as those mutations (orange) and mutations all other residues (gray). Dotted line and score indicate optimal threshold for each predictor on known the validation set.

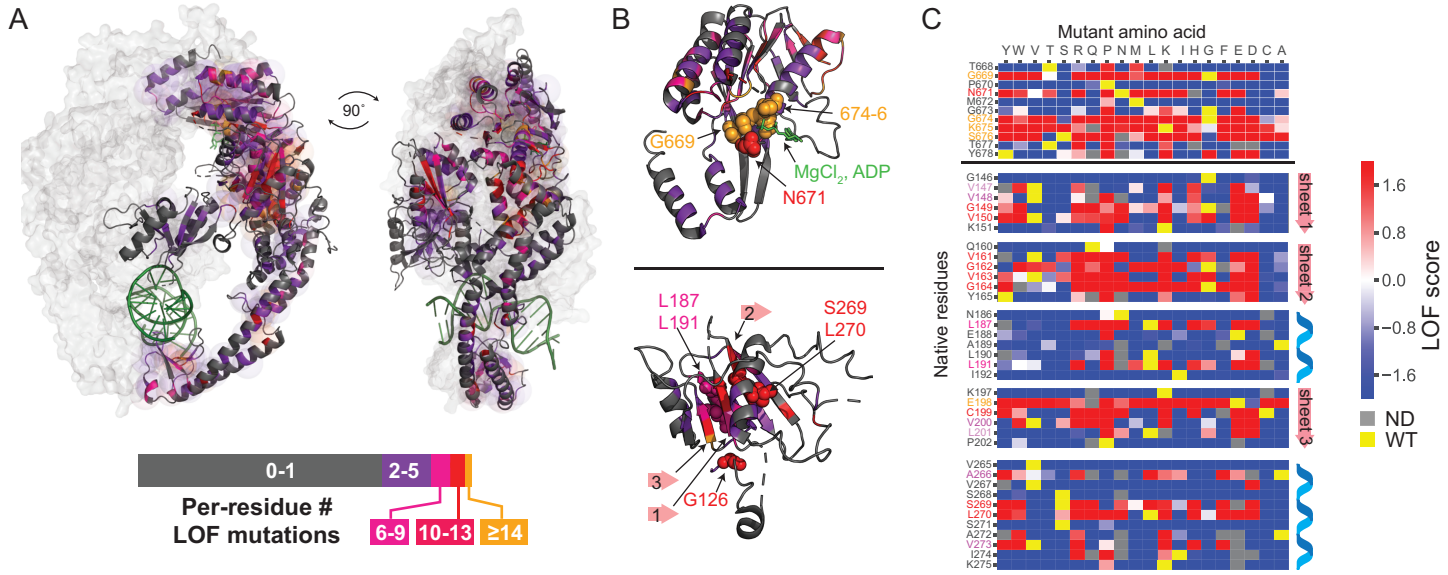

Figure 5. Structural insights from deep mutational scanning data. (A) MutSα crystal structure (PDB:2O8E), with MSH6 surface in light gray, and MSH2 shaded by the number of deleterious missense

567 variants at each (length of bar in legend proportional to count of residues with denoted range of LOF
568 mutations). (B) Extreme intolerance to substitution in MSH2 ATPase domain (upper), and connector
569 domains (lower); selected residues or beta sheets shown with spheres or arrows, respectively. (C) LOF
570 score heatmap (as in Figure 2C) showing mutational intolerance at Walker A motif of the ATPase domain
571 (upper) and selected connector domain residues (lower) corresponding to (B).

572